SCIENCE CHINA
Information Sciences

• **Supplementary File** •

Distributed Periodic Event-Triggered Terminal Sliding Mode Control for Vehicular Platoon System

Mengjie Li[1], Shaobao Li[1], Xiaoyuan Luo[1*], Xinquan Zheng[1] & Xinping Guan[2]

[1]*School of Electrical Engineering, Yanshan University, Qinhuangdao* 066004*, China;*
[2]*School of Electronic, Information and Electrical Engineering, Shanghai Jiao Tong University, Shanghai* 200240*, China*

Appendix A Literature review

In recent years, there has been a growing interest in the platooning of vehicular systems as a means of alleviating severe traffic issues. The cornerstone of a vehicular platoon system is wireless inter-vehicle communication, i.e., VANETs, which allows vehicles to share useful information such as position, velocity, and acceleration with their neighbors. This abundant information enables the deployment of advanced algorithms and driving in a compact inter-vehicle spacing for reduced air resistance and increased traffic capacity. However, a large number of vehicles occupying the communication channel can impose a significant burden on the communication system, resulting in undesired communication issues. Moreover, as the platoon scale and traffic density increase, there is a growing need for vehicles to have strong anti-interference capabilities.

Traditionally, most research on vehicular platooning has been based on a time-triggered mechanism (TTM), which requires data transmission among successive vehicles at fixed periodic sampling intervals. However, this approach relies solely on time rather than the actual status of the vehicles [1], and is often wasteful of communication resources when the platoon system is stable and vehicular state changes are insignificant [2]. To address this issue, an event-triggered mechanism (ETM) has emerged as an alternative. With ETM, data is transmitted only when a triggering condition is met, such as when the changes in vehicle status exceed a preset threshold. This can greatly reduce transmission frequency and save communication resources [3]. Several studies have investigated event-triggered mechanisms for vehicular platooning, including a proposed communication scheme in [1] to reduce the occupation of communication resources while maintaining string stability, and the dynamic event-triggered mechanism (DETM) in [4], [5] that adjust the triggered threshold according to both vehicular status and an additional internal variable to occupy fewer communication resources than traditional ETM. However, continuous measurement of system states is required to determine triggering instants, which may be challenging to deploy in a time-sliced software platform. An alternative approach, periodic event-triggered mechanism (PETM), has received extensive attention as it monitors the status periodically without requiring continuous measurement. Despite this, there is still limited research on the application of PETM in vehicular platoon systems.

However, the aforementioned event-triggered mechanisms require the continuous measurement of system states to determine triggering instants, which may be hard to deploy in the time-sliced software platform [6]. As an alternative, PETM monitors the status periodically without continuous measurement and has received extensive attention [7–9]. To the best of authors' knowledge, there is few research on periodic event-triggered mechanism for vehicular platoon system.

Compared to TTM-based vehicular systems, those based on ETM are more vulnerable to perturbations due to reduced real-time data communication. Therefore, anti-interference measures are critical for ensuring the reliability of vehicular systems. Sliding mode control (SMC), an important robust control method, has been extensively developed for vehicular platoon systems [10–14]. Researchers have developed a distributed integral sliding mode approach combined with neural network techniques for vehicular systems [10], which was extended to the proportional-integral-derivative sliding mode case [11]. However, the aforementioned linear sliding mode approaches can only guarantee asymptotic convergence, which may take infinite time to achieve. To overcome this limitation, a terminal sliding mode strategy was presented for vehicular platoons [12], ensuring finite-time stability. Nevertheless, these methods require continuous inter-vehicle communication, leading to a waste of communication resources. Therefore, ensuring robustness while saving communication resources is still an open problem in the field of vehicular platoon systems. To achieve communication economy and robust performance simultaneously, the ETM-based SMC approach has gained considerable attention in various fields [15–17]. For instance, researchers have designed an ETM-based distributed SMC approach in [15] to decrease the controller sampling frequency. However, this requires continuous communication among agents and may violate the original intention of ETM. In [16], a PETM using SMC was proposed to achieve robust performance for a single linear time-invariant system and was extended to a permanent-magnet synchronous motor [17]. Nevertheless, there is limited research on PETM-based distributed SMC strategies, especially for vehicular platoon systems.

The SMC method typically involves a switching function, and robustness requires the switching gain to exceed the disturbance magnitude [18]. However, a larger gain can cause chattering, which may harm the actuators and systems. Additionally, the exact disturbance bound is often unknown in practice. To address this issue, many studies have applied extended state observers (ESO) [19–22]. In [21], a second-order sliding mode control combined with ESO was applied to a small-scale helicopter with smaller switching gain. The similar concept was applied to an interconnected power system in [22]. Nevertheless, the aforementioned ESOs can only achieve asymptotic convergence and require the continuous communication. Recently, the finite-time extended state observer has gained attention in many fields [23–25] and an ETM-based ESO was proposed in [26] which motivate this research.

In vehicular platoon systems, string stability is critical, ensuring that inter-vehicle spacing errors will not enlarge along the platoon [27, 28]. Considerable attention has been given to string stability over the past few decades, and most studies rely on the Constant Time Headway (CTH) policy [29, 30]. However, guaranteed string stability methods typically overlook traffic flow stability, and the CTH policy cannot ensure TFS [31]. Traffic flow stability characterizes the evolution of the average velocity

* Corresponding author (email: xyluo@ysu.edu.cn)

and traffic density as they respond to changes in traffic density [32]. When TFS is violated, even a small density variation will impact each vehicle in the platoon, and less flow can pass through [33]. The reduced flow can lead to traffic inefficiency, even causing congestion. By means of the aforementioned discussions, how to guarantee the string stability and traffic flow stability simultaneously motivates this article.

Appendix B Selection of the EFESO Parameters

To obtain satisfactory observation performance, ε is set as a positive constant and α_i satisfies $\alpha_i \in (2/3, 1)$. The gain k_j^i is the constant such that the following matrix A_i is Hurwitz.

$$A_i = \begin{bmatrix} k_1^i & 1 & 0 & 0 \\ k_2^i & 0 & 1 & 0 \\ k_3^i & 0 & 0 & 1 \\ k_4^i & 0 & 0 & 0 \end{bmatrix}. \tag{B1}$$

To obtain the parameter k_j^i, we introduce the following Lemma.

Lemma 1 ([34]). Consider the following matrixs

$$A = \begin{bmatrix} 0_{(n-1)\times 1} & I_{n-1} \\ 0 & 0_{1\times(n-1)} \end{bmatrix} \in R^{n\times n}, C = \begin{bmatrix} 1, & 0_{1\times(n-1)} \end{bmatrix} \in R^{1\times n}, K = \begin{bmatrix} k_1^i & \cdots & k_n^i \end{bmatrix}^T \in R^{n\times 1}.$$

Since the pair of (A, C) is observable, the eigenvalues $\lambda = \{\lambda_j\}$ of the matrix $A - KC$ can be assigned by designing the gain matrix K as follows. Step 1. Select λ, where each element λ_j in λ is not equal. Step 2. Select the gain matrix K as $K = -V^{-1}(\lambda)\begin{bmatrix} \lambda_1^n & \cdots & \lambda_n^n \end{bmatrix}^{\mathrm{T}}$ where the Vandermonde matrix $V(\lambda)$ is defined as

$$V(\lambda) = \begin{bmatrix} \lambda_1^{n-1} & \cdots & \lambda_1 & 1 \\ \vdots & \ddots & \vdots & \vdots \\ \lambda_n^{n-1} & \cdots & \lambda_n & 1 \end{bmatrix}.$$

Then the matrix can be diagonalised by the matrix $A - KC$ and the following equation can be obtained $V(\lambda)\,(A - KC)\,V^{-1}(\lambda) = \mathrm{diag}\,\{\lambda_j\} = \Lambda$, whicequals $A - KC = V^{-1}(\lambda)\Lambda V(\lambda)$. The above statement indicates that if n=4, then the matrix $A - KC$ equals A_i in (B1) which means a hurwitz matrix A_i can be obtained.

Appendix C Proof of Theorem 1

In order to analyse the finite-time convergence of the PFESO, the definitions of homogeneity and some lemmas are introduced as follows.

Definition 1. ([35]) A function $V(\chi) : R^n \to R$ is termed as homogeneous of degree d relative to weights $\{\iota_i > 0\}_{i=1}^n$, if

$$V\left(\lambda^{\iota_1}\chi_1, \lambda^{\iota_2}\chi_2, \ldots, \lambda^{\iota_n}\chi_n\right) = \lambda^d V(\chi_1, \chi_2, \ldots, \chi_n) \tag{C1}$$

for all $\lambda > 0$ and $\chi = (\chi_1, \chi_2, \ldots, \chi_n) \in R^n$. If V satisfies (C1) and is differentiable with respect to χ_n, then the partial derivative of V in χ_n follows

$$\lambda^{\iota_n}\frac{\partial}{\partial\chi_n}V\left(\lambda^{\iota_1}\chi_1, \ldots, \lambda^{\iota_n}\chi_n\right) = \lambda^d\frac{\partial}{\partial\chi_n}V(\chi_1, \ldots, \chi_n) \tag{C2}$$

Definition 2. ([35]) A vector field $F(\chi) : R^n \to R$ is termed as homogeneous of degree d relative to weights $\{\iota_i > 0\}_{i=1}^n$, if the ith component of F satisfies

$$F_i\left(\lambda^{\iota_1}\chi_1, \lambda^{\iota_2}\chi_2, \ldots, \lambda^{\iota_n}\chi_n\right) = \lambda^{\iota_i + d}F_i(\chi_1, \chi_2, \ldots, \chi_n) \tag{C3}$$

for all $\lambda > 0$ and $\chi = (\chi_1, \chi_2, \ldots, \chi_n) \in R^n$.

Lemma 2. (Tube lemma [36]) Consider a product space $X \times Y$ where Y is compact. If N is an open set of $X \times Y$ containing the slice $\{x_0\} \times X$ of $X \times Y$, then N contains some tube $W \times Y$ about $\{x_0\} \times Y$, where W is a neighborhood of x_0 in X.

Lemma 3. ([36])Consider the continuous real-valued functions V_1, V_2 on R^n, and be homogeneous of degree $\iota_1 > 0$, $\iota_2 > 0$ with respect to ν, where V_1 is positive definite. Then, the following inequality holds for any $\chi \in R^n$,

$$\left[\min\nolimits_{\{z:V_1(z)=1\}}V_2(z)\right]\left[V_1(\chi)\right]^{\frac{\iota_2}{\iota_1}} \leqslant V_2(\chi) \leqslant \left[\max\nolimits_{\{z:V_1(z)=1\}}V_2(\chi)\right]\left[V_1(\chi)\right]^{\frac{\iota_2}{\iota_1}}. \tag{C4}$$

Lemma 4. ([37])Suppose a function f satisfies $f \in C(R^n, R^n)$ and $f(0) = 0$; for any positive constant λ, f is homogeneous and $f_i\left(\lambda^{\iota_1}\chi_1, \lambda^{\iota_2}\chi_2, \ldots, \lambda^{\iota_n}\chi_n\right) = \lambda^{d+\iota_i}f_i(\chi_1, \chi_2, \ldots, \chi_n)$, where $\tau \in R$; and the trivial solution $\chi = 0$ of $\dot{\chi} = f(\chi)$ is locally asymptotically stable. Consider a positive integer μ and a real number ν satisfied $\nu > \mu \cdot \max_{1\leqslant i\leqslant n}\iota_i$. Then, there exists a function $V : R^n \to R$ such that: (a) $V \in C^p(R^n, R) \cap C^\infty(R\backslash\{0\}, R)$; (b) $V(0) = 0, V(\chi) > 0$ for any $\chi \neq 0$ and $V(\chi) \to +\infty$ as $\|\chi\| \to +\infty$; (c) V is homogeneous for $\forall\lambda > 0$: $V\left(\lambda^{\iota_1}\chi_1, \lambda^{\iota_2}\chi_2, \ldots, \lambda^{\iota_n}\chi_n\right) = \lambda^\nu V(\chi_1, \chi_2, \ldots, \chi_n)$; (d) for $\forall\chi \neq 0$, $\nabla V(\chi) \cdot f(\chi) < 0$.

Lemma 5. ([38])The following conditions are equivalent for the system $\dot{\chi} = f(\chi, u)$:

1). $\dot{\chi} = f(\chi, u)$ is finite-time input-to-state stable (ISS) with the input u.

2). There exists a positive-definite Lyapunov function $V(\chi)$ such that

$$\dot{V} \leqslant -\mu_1(V) + \mu_2\left(\|u\|\right), \tag{C5}$$

where μ_1, μ_2 are K_∞ functions, and $|\mu_1| \leqslant \alpha \left|V^\beta\right|$ as $V \to 0$ for a constant $\beta \in (0,1)$.

3). $\dot{\chi} = f(\chi, u)$ is (weakly) finite-time robustly stable.

Denote the estimation errors as

$$\begin{cases} \tilde{x}_i = \hat{x}_i - x_i(t), \eta_1^i = \frac{\tilde{x}_i(\varepsilon t)}{\varepsilon^3} \\ \tilde{v}_i = \hat{v}_i - v_i(t), \eta_2^i = \frac{\tilde{v}_i(\varepsilon t)}{\varepsilon^2} \\ \tilde{a}_i = \hat{a}_i - a_i(t), \eta_3^i = \frac{\tilde{a}_i(\varepsilon t)}{\varepsilon} \\ \tilde{w}_i = \hat{w}_i - w_i(t), \eta_4^i = \tilde{w}_i(\varepsilon t) \end{cases}. \tag{C6}$$

Based on (2), (4) and (C6), the estimation error dynamics of PFESO can be obtained as

$$\begin{cases} \dot{\eta}_1^i = \eta_2^i + k_1^i \lceil \eta_1^i \rfloor^{\alpha_i} + k_1^i \beta_1^i \\ \dot{\eta}_2^i = \eta_3^i + k_2^i \lceil \eta_1^i \rfloor^{2\alpha_i - 1} + k_2^i \beta_2^i \\ \dot{\eta}_3^i = \eta_4^i + k_3^i \lceil \eta_1^i \rfloor^{3\alpha_i - 2} + k_3^i \beta_3^i + \left(a_i - a_i\left(t_k^i\right)\right)/\tau_i \\ \dot{\eta}_4^i = k_4^i \lceil \eta_1^i \rfloor^{4\alpha_i - 3} + k_4^i \beta_4^i - \varepsilon \dot{w}_i \end{cases}, \tag{C7}$$

where $\beta_1^i = \lceil \eta_1^i - \bar{x}_i/\varepsilon^3 \rfloor^{\alpha_i} - \lceil \eta_1^i \rfloor^{\alpha_i}$, $\beta_2^i = \lceil \eta_1^i - \bar{x}_i/\varepsilon^3 \rfloor^{2\alpha_i - 1} - \lceil \eta_1^i \rfloor^{2\alpha_i - 1}$, $\beta_3^i = \lceil \eta_1^i - \bar{x}_i/\varepsilon^3 \rfloor^{3\alpha_i - 2} - \lceil \eta_1^i \rfloor^{3\alpha_i - 2}$, $\beta_4^i = \lceil \eta_1^i - \bar{x}_i/\varepsilon^3 \rfloor^{4\alpha_i - 3} - \lceil \eta_1^i \rfloor^{4\alpha_i - 3}$ and $\bar{x}_i = x_i\left(t_k^i\right) - x_i(t)$. Note that functions $f_1^i(y) = \lceil y \rfloor^{\alpha_i}$, $f_2^i(y) = \lceil y \rfloor^{2\alpha_i - 1}$, $f_3^i(y) = \lceil y \rfloor^{3\alpha_i - 2}$, $f_4^i(y) = \lceil y \rfloor^{4\alpha_i - 3}$ are Lipschitz. Therefore, we have

$$\left\|\beta_j^i\right\| = \left\|f_j^i\left(\eta_1^i - \bar{x}_i/\varepsilon^3\right) - f_j^i\left(\eta_1^i\right)\right\| \leqslant l_j^i \left\|\bar{x}_i\right\|. \tag{C8}$$

Proof. Before analyzing the stability of system (C7), consider the following system

$$\dot{\eta}_i = \Phi_i(\eta_i) \tag{C9}$$

where $\eta^i = \left[\eta_1^i, \eta_2^i, \eta_3^i, \eta_4^i\right]^T$ and

$$\Phi_i(\eta_i) = \begin{bmatrix} \eta_2^i + k_1^i \lceil \eta_1^i \rfloor^{\alpha_i} \\ \eta_3^i + k_2^i \lceil \eta_1^i \rfloor^{2\alpha_i - 1} \\ \eta_4^i + k_3^i \lceil \eta_1^i \rfloor^{3\alpha_i - 2} \\ k_4^i \lceil \eta_1^i \rfloor^{4\alpha_i - 3} \end{bmatrix} \tag{C10}$$

If $\alpha_i = 1$, (C9) becomes

$$\dot{\eta}_i = A_i \eta_i, \tag{C11}$$

which is asymptotically stable when the matrix A_i is Hurwitz. Then, consider a proper function $V_1^i(\alpha_i, \eta_i)$ and a compact set $S_i = \left\{\eta_i \in R^4 : V_1^i(1, \eta_i) = 1\right\}$. Further, define a function $\varphi_i : R^+ \times S_i \to R : (\alpha_i, \eta_i) \to \dot{V}_1^i$. Note that φ_i is continuous, then the $\varphi_i^{-1}\left(R^-\right)$ is an open subset of $\Lambda \times S_i$ which contains the slice $\{1\} \times S_i$. Since S_i is compact, it can be derived from the Lemma 1 that $\varphi_i^{-1}\left(R^-\right)$ contains the tube $\left(1 - \underline{\varepsilon}_i, 1 + \bar{\varepsilon}_i\right) \times S_i$. Evidently, for any $(\alpha_i, \eta_i) \in \left(1 - \underline{\varepsilon}_i, 1 + \bar{\varepsilon}_i\right) \times S_i$, one has $\dot{V}_1^i < 0$. Therefore, the origin of (C9) is locally asymptotically stable.

Then, the finite-time ISS of estimation error dynamics (C7) will be presented in the following step. The vector field Φ_i in (C10) is homogeneous of degree $\alpha_i - 1$ with respect to the weights $\{1, \alpha_i, 2\alpha_i - 1, 3\alpha_i - 2\}$. Meanwhile, system (C9) is locally asymptotically stable. From the Lemma 3, there exists a positive definite, radially unbounded function $V_2^i(\eta_i) : R^4 \to R$ such that $V_2^i(\eta_i)$ is homogeneous of degree γ_i with respect to the weights $\{1, \alpha_i, 2\alpha_i - 1, 3\alpha_i - 2\}$, and $\frac{\partial V_2^i}{\partial \eta_1^i}\left(\eta_2^i + k_1^i \lceil \eta_1^i \rfloor^{\alpha_i}\right) + \frac{\partial V_2^i}{\partial \eta_2^i}\left(\eta_3^i + k_2^i \lceil \eta_1^i \rfloor^{2\alpha_i - 1}\right) + \frac{\partial V_2^i}{\partial \eta_3^i}\left(\eta_4^i + k_3^i \lceil \eta_1^i \rfloor^{3\alpha_i - 2}\right) + \frac{\partial V_2^i}{\partial \eta_4^i}\left(k_4^i \lceil \eta_1^i \rfloor^{4\alpha_i - 3}\right)$ is negative definite and homogeneous of degree $\gamma_i + \alpha_i - 1$. According to the homogeneity of $V_2^i(\eta_i)$, it can be obtained that $\left|\frac{\partial V_2^i}{\partial \eta_1^i}\right|$ is homogeneous of degree $\gamma_i - 1$, $\left|\frac{\partial V_2^i}{\partial \eta_2^i}\right|$ is homogeneous of degree $\gamma_i - \alpha_i$, $\left|\frac{\partial V_2^i}{\partial \eta_3^i}\right|$ is homogeneous of degree $\gamma_i - 2\alpha_i + 1$ and $\left|\frac{\partial V_2^i}{\partial \eta_4^i}\right|$ is homogeneous of degree $\gamma_i - 3\alpha_i + 2$. From Lemma 2 and Lemma 3, it can be conclued that

$$\begin{aligned} &\frac{\partial V_2^i}{\partial \eta_1^i}\left(\eta_2^i + k_1^i \lceil \eta_1^i \rfloor^{\alpha_i}\right) + \frac{\partial V_2^i}{\partial \eta_2^i}\left(\eta_3^i + k_2^i \lceil \eta_1^i \rfloor^{2\alpha_i - 1}\right) + \frac{\partial V_2^i}{\partial \eta_3^i}\left(\eta_4^i + k_3^i \lceil \eta_1^i \rfloor^{3\alpha_i - 2}\right) \\ &+ \frac{\partial V_2^i}{\partial \eta_4^i}\left(k_4^i \lceil \eta_1^i \rfloor^{4\alpha_i - 3}\right) \leqslant -\mu_1^i\left(V_2^i\right)^{\frac{\gamma_i + \alpha_i - 1}{\gamma_i}}, \end{aligned} \tag{C12}$$

and

$$\begin{cases} \left|\frac{\partial V_2^i}{\partial \eta_1^i}\right| \leqslant \mu_2^i\left(V_2^i\right)^{\frac{\gamma_i - 1}{\gamma_i}} \\ \left|\frac{\partial V_2^i}{\partial \eta_2^i}\right| \leqslant \mu_3^i\left(V_2^i\right)^{\frac{\gamma_i - \alpha_i}{\gamma_i}} \\ \left|\frac{\partial V_2^i}{\partial \eta_3^i}\right| \leqslant \mu_4^i\left(V_2^i\right)^{\frac{\gamma_i - 2\alpha_i + 1}{\gamma_i}} \\ \left|\frac{\partial V_2^i}{\partial \eta_4^i}\right| \leqslant \mu_5^i\left(V_2^i\right)^{\frac{\gamma_i - 3\alpha_i + 2}{\gamma_i}} \end{cases}, \tag{C13}$$

where μ_j^i, $j=1,\cdots,5$, are positive constants. Then, the derivative of $V_2^i(\eta_i)$ can be derived as

$$\begin{aligned}\dot{V}_{i1} =& \frac{\partial V_{i1}}{\partial\eta_1^i}\left(\eta_2^i + k_1^i\lceil\eta_1^i\rfloor^{\alpha_i}\right) + \frac{\partial V_{i1}}{\partial\eta_2^i}\left(\eta_3^i + k_2^i\lceil\eta_1^i\rfloor^{2\alpha_i-1}\right) + \frac{\partial V_{i1}}{\partial\eta_3^i}\left(\eta_4^i + k_3^i\lceil\eta_1^i\rfloor^{3\alpha_i-2}\right) + \frac{\partial V_{i1}}{\partial\eta_4^i}\left(k_4^i\lceil\eta_1^i\rfloor^{4\alpha_i-3} - \varepsilon\dot{w}_i\right)\\ &+ \frac{\partial V_{i1}}{\partial\eta_1^i}k_1^i\beta_1^i + \frac{\partial V_{i1}}{\partial\eta_2^i}k_2^i\beta_2^i + \frac{\partial V_{i1}}{\partial\eta_4^i}k_4^i\beta_4^i + \frac{\partial V_{i1}}{\partial\eta_3^i}\left(k_3^i\beta_3^i + \left(a_i - a_i\left(t_k^i\right)\right)/\tau_i\right)\\ \leqslant& -\mu_5^i(V_{i1})^{\frac{\gamma_i+\alpha_i-1}{\gamma_i}} + k_1^i\mu_1^i(V_{i1})^{\frac{\gamma_i-1}{\gamma_i}}l_1^i\bar{\delta}_i + k_2^i\mu_2^i(V_{i1})^{\frac{\gamma_i-\alpha_i}{\gamma_i}}l_2^i\bar{\delta}_i + \mu_3^i\left(k_3^il_3^i\bar{\delta}_i + \tau_i^{-1}\bar{\delta}_i\right)(V_{i1})^{\frac{\gamma_i-2\alpha_i+1}{\gamma_i}}\\ &+ \left(k_4^il_4^i\bar{\delta}_i + \varepsilon w_m\right)\mu_4^i(V_{i1})^{\frac{\gamma_i-3\alpha_i+2}{\gamma_i}}.\end{aligned} \tag{C14}$$

As

$$\|\eta_i\| \geqslant \max\left\{V_{i1}^{-1}\left(\frac{k_1^i\mu_1^il_1^i\bar{\delta}_i}{\mu_5^i\theta_i^1}\right)^{c_1}; V_{i1}^{-1}\left(\frac{k_2^i\mu_2^il_2^i\bar{\delta}_i+\tau_i^{-1}\bar{\delta}_i}{\mu_5^i\theta_2^i}\right)^{c_2}; V_{i1}^{-1}\left(\frac{k_3^i\mu_3^il_3^i\bar{\delta}_i}{\mu_5^i\theta_3^i}\right)^{c_3}; V_{i1}^{-1}\left(\frac{k_4^i\mu_4^il_4^i\bar{\delta}_i+\mu_4^i\varepsilon w_m}{\mu_5^i\theta_4^i}\right)^{c_4}\right\} \tag{C15}$$

renders

$$\dot{V}_{i1} \leqslant -\mu_5^i\left(1-\theta_1^i-\theta_2^i-\theta_3^i-\theta_4^i\right)V_{i1}(\eta_i)^{\frac{\gamma_i+\alpha_i-1}{\gamma_i}}, \tag{C16}$$

where $c_1 = \frac{\gamma_i-1}{\gamma_i+\alpha_i-1}, c_2 = \frac{\gamma_i-\alpha_i}{\gamma_i+\alpha_i-1}$, $c_3 = \frac{\gamma_i-2\alpha_i+1}{\gamma_i+\alpha_i-1}$, $c_4 = \frac{\gamma_i-3\alpha_i+2}{\gamma_i+\alpha_i-1}$ and $0 < \theta_1^i+\theta_2^i+\theta_3^i+\theta_4^i < 1$. According to Lemma 4, the error system (C7) is finite-time input-to-state stable, and

$$\|\eta_i(t)\| \leqslant \max\left\{\varpi\left(\|\eta_i(0)\|, t\right), \varphi_1\left(\bar{\delta}_i\right), \varphi_2\left(\bar{\delta}_i\right), \varphi_3\left(\bar{\delta}_i\right), \varphi_4\left(\bar{\delta}_i+w_m\right)\right\} \tag{C17}$$

where φ_i is a $\mathscr{K}$ function and ϖ_i is a $\mathscr{KL}$ function with $\varpi_i\left(\eta_i(0), t\right) \equiv 0$ when $t > T$ for a settled time $T\left(\eta_i(0)\right) \leqslant \gamma_i\left(V_{i1}\left(\eta_i(0)\right)\right)^{\frac{1-\alpha_i}{\gamma_i}} \Big/ \left(\mu_5^i\left(1-\alpha_i\right)\left(1-\sum_{j=1}^{4}\theta_j^i\right)\right)$.

Appendix D Effectiveness of coupled quadratic spacing strategy

The coupled quadratic spacing error depicts the relationship between the spacing errors of the vehicular platoon. It is not difficult to find that the string stability can be guaranteed if the term $\lim_{t\to t_c}\varepsilon_i(t) = 0$ holds. The following lemma shows the relationship between ε_i and e_i.

Lemma 6. Equation $\lim_{t\to t_c}\varepsilon_i(t) = 0$ is equivalent to $\lim_{t\to t_c}e_i(t) = 0$ for $i = 1, 2\cdots N$.

Proof. Writing ε_i and e_i in the vector form $\varepsilon = [\varepsilon_1, \varepsilon_2\cdots\varepsilon_N]^T$ and $e = [e_1, e_2\cdots e_N]^T$ yields

$$\varepsilon = \gamma e, \tag{D1}$$

where

$$\gamma = \begin{bmatrix}\gamma_1 & -1 & \cdots & 0\\ 0 & \gamma_2 & \cdots & 0\\ \vdots & \vdots & \ddots & \vdots\\ 0 & 0 & \cdots & \gamma_N\end{bmatrix}.$$

Since γ_i, $i = 1, 2\cdots N$ are postive constants, we have that matrix γ is a nonsingular matrix, which directly deduces the conclusion. The proof is thus completed.

Appendix E Estimation of Upper Bound for δ_i

It is noted that the PETM can only monitor the triggered condition at a predesigned period λ_i. This means that the actual bound of triggered error δ_i may exceed $\bar{\delta}_i$ between two consecutive sampled instants [16], [17]. By considering a worst case, the upper bound of δ_i is given in the following lemma.

Lemma 7. Consider the vehicular platoon system (1) and (2), the PETM (3) and the control law (7), the triggered error δ_i satisfies

$$\|\delta_i(t)\| \leqslant \left(\bar{\delta}_i + \left(L_1^i\right)^{-1}\left(\left\|h_i\left(t_k^i\right)\right\| + \bar{w}_m^i\right)\right)e^{L_1^i\lambda_i} - \left(L_1^i\right)^{-1}\left(\left\|h_i\left(t_k^i\right)\right\| + \bar{w}_m^i\right), \tag{E1}$$

where L_1^i is a Lipschitz constant and $\bar{w}_m^i = \max\left\{\tilde{w}_i(t)\right\}$ is bounded by Theorem 1, and $h_i(t)$ is a vector function defined as

$$h_i(t) = \begin{bmatrix}\dot{e}_i(t)\\ a_i(t)\\ -\tau_i^{-1}a_i(t) + \gamma_i^{-1}\mathcal{G}_i(t) + k_i\vartheta_i^{-1}g_i^{-1}\mathrm{sgn}\left(s_i\right)\end{bmatrix}, \tag{E2}$$

where $\mathcal{G}_i(t) \triangleq \beta_i^{-1}p_i^{-1}g_i^{-1}\dot{\varepsilon}_i^{2-p_i} + g_i^{-1}\varpi_i$.

Proof. In order to research the evolution of $\delta_i(t)$, consider the differential inequality of it during the time interval $\left[t_k^i + (j_i-1)\lambda_i, t_k^i + j_i\lambda_i\right)$.

$$\frac{d\|\delta_i(t)\|}{dt} \leqslant \left\|\dot{\delta}_i(t)\right\| = \left\|\begin{bmatrix}\dot{e}_i(t) - \dot{e}_i\left(t_k^i\right)\\ a_i(t) - a_i\left(t_k^i\right)\\ -\tau_i^{-1}a_i(t) + \tau_i^{-1}a_i\left(t_k^i\right)\end{bmatrix} + \begin{bmatrix}0\\ 0\\ w_i(t) - \hat{w}_i\left(t_k^i\right)\end{bmatrix} + h_i\left(t_k^i\right)\right\| \tag{E3}$$

Denote the function $f_i[\xi_i(t)] \triangleq \left[\dot{e}_i(t), a_i(t), -\tau_i^{-1}a_i(t)\right]$, since $f_i[\xi_i(t)]$ is Lipschitz, then, we have $f_i[\xi_i(t)] - f_i\left[\xi_i\left(t_k^i\right)\right] \leqslant L_1^i \left\|\xi_i(t) - \xi_i\left(t_k^i\right)\right\| \leqslant L_1^i\|\delta_i\|$. To obtain the upper bound of $\delta_i(t)$, we consider the worst possible case: The event (3) is violated immediately after $t_k^i + (j_i-1)\lambda_i$, which means that $\lim\limits_{\Delta t \to 0^+} \delta_i\left(t_k^i + (j_i-1)\lambda_i + \Delta t\right) = \bar{\delta}_i$. By means of the aforementioned initial condition and Comparison lemma, the solution to (E3) can be derived as

$$\|\delta_i(t)\| \leqslant \left(\left(L_1^i\right)^{-1}\left(\left\|h_i\left(t_k^i\right)\right\| + \bar{w}_m^i\right)\right)e^{L_1^i\left(t - t_k^i - (j_i-1)\lambda_i\right)} - \left(L_1^i\right)^{-1}\left(\left\|h_i\left(t_k^i\right)\right\| + \bar{\delta}_i + \bar{w}_m^i\right) \tag{E4}$$

Notice that the exponential function increases monotonously with t in the interval $\left[t_k^i + (j_i-1)\lambda_i, t_k^i + j_i\lambda_i\right)$. It means that the triggered error $\|\delta_i(t)\|$ reaches the maximum value at the instant $t = t_k^i + j_i\lambda_i$. Consequently, the inequality (E1) is derived and the proof is completed.

Remark 1. When the sampling period λ_i tends to zero, i.e., the continuous measurements case, the PETM (3) will degrade into the static event triggered mechanism (SETM) as in [4], [5], [39]. In the meanwhile, the upper bound of $\|\delta_i(t)\|$ tends to $\bar{\delta}_i$, which shows that the SETM is a special case of the PETM.

Remark 2. It is worth mentioned that the triggered error $\|\delta_i(t)\|$ increases with the sampling period λ_i, which is intuitive. At the meantime, it provides guidance for the design of the sampling period.

Appendix F Basis for the selection of λ_i

The sampling period λ_i is the foundation for the PETM and involves the stability of systems. When the sampling period is small, the PETM will degrade into continuous-time measurement and may be hard to deploy in practice. On the other hand, the large λ_i can corrode the performance as shown in Lemma 6. So, in this section, a selection criterion of λ_i is proposed for the PETM as follows.

First, it is necessary to derive the upper bound of the function $h_i(t)$ in (E2), by resorting to (7) and Assumption 2, one has

$$\|h_i(t)\| \leqslant \vartheta_i^{-1}q_i^{-1}\left[(\gamma_i+1)(v_m + q_i a_m + r_i v_m a_m) + k_i + 1\right] + \tau_i^{-1}a_m \triangleq \bar{h}_i \tag{F1}$$

Now, the selection criterion of the sampling period λ_i is given as

$$0 < \lambda_i < \bar{\lambda}_i, \tag{F2}$$

where $\bar{\lambda}_i = \frac{1}{L_1^i}\ln\left(1 + \frac{\sigma_i}{(L_1^i)^{-1}(\bar{h}_i + \bar{w}_m^i) + \bar{\delta}_i}\right)$ with a specified constant σ_i. Then, according to the sampling period (F2), the upper bound of δ_i can be obtained from (E1) that

$$\|\delta_i(t)\| \leqslant \bar{\delta}_i e^{L_1^i\lambda_i} + \left(L_1^i\right)^{-1}\left(\bar{h}_i + \bar{w}_m^i\right)\left(e^{L_1^i\lambda_i} - 1\right) = \bar{\delta}_i + \sigma_i. \tag{F3}$$

Appendix G Proof of Theorem 2

In this appendix, the reachability of practical sliding mode is analyzed for the specified terminal sliding surface (6) at first and then the ultimately boundedness of the platoon system is derived under the controller (7). Finally, by means of the ultimately boundedness and the coupled quadratic spacing strategy, the TFS and string stability are guaranteed simultaneously.

Appendix G.1 Reachability of Practical Sliding Mode

Proof. For each vehicle, consider the Lyapunov function candidate $V_i(t) = \frac{1}{2}s_i^2(t)$. Differentiating $V_i(t)$ with respect to time, it derives

$$\dot{V}_i(t) = s_i(t)\dot{s}_i(t) = s_i(t)\beta_i p_i g_i \dot{\varepsilon}_i^{p_i-1}\left(\mathcal{G}_i(t) - \frac{\gamma_i}{\tau_i m_i}u_i - \gamma_i w_i\right) \tag{G1}$$

Substituting the control law (7), one obtains

$$\dot{V}_i(t) = s_i(t)\beta_i p_i g_i \dot{\varepsilon}_i^{p_i-1}\left(\mathcal{G}_i(t) - \mathcal{G}_i\left(t_k^i\right) - \gamma_i\tilde{w}_i - \beta_i^{-1}p_i^{-1}g_i^{-1}\left(t_k^i\right)k_i \operatorname{sgn}\left(s_i\left(t_k^i\right)\right)\right). \tag{G2}$$

Considering $\mathcal{G}_i(t)$ is Hölder continuous, the following inequality can be obtained as

$$\left\|\mathcal{G}_i(t) - \mathcal{G}_i\left(t_k^i\right)\right\| \leqslant L_2^i\left\|\Xi_i(t) - \Xi_i\left(t_k^i\right)\right\|^r \leqslant L_2^i\left(\sqrt{\sum_{j=i-1}^{i+1}\bar{\delta}_j^2}\right)^r, \tag{G3}$$

where L_2^i is a positive Hölder constant and $\Xi_i(t) = [\xi_{i-1}(t), \xi_i(t), \xi_{i+1}(t)]$. Now, the reachability of practical sliding mode can be proved in two steps: (i) the states of system have not reached practical sliding mode, i.e., $\operatorname{sgn}\left(s_i\left(t_k^i\right)\right) = \operatorname{sgn}(s_i(t))$; (ii) the states of system have reached practical sliding mode and will remain in this region, i.e., $\operatorname{sgn}\left(s_i\left(t_k^i\right)\right) \neq \operatorname{sgn}(s_i(t))$.

- When $\operatorname{sgn}\left(s_i\left(t_k^i\right)\right) = \operatorname{sgn}(s_i(t))$ holds for $t \in \left[t_k^i, t_k^{i+1}\right)$, it can be derived from (G2) that

$$\dot{V}_i \leqslant \beta_i p_i g_i \dot{\varepsilon}_i^{p_i-1}|s_i(t)|\left(L_2^i\left(\sqrt{\sum_{j=i-1}^{i+1}\bar{\delta}_j^2}\right)^r + \gamma_i\bar{w}_m^i - \beta_i^{-1}p_i^{-1}g_i^{-1}\left(t_k^i\right)k_i\right) \tag{G4}$$

In the follows, two subcases are discussed.

(1) When $\dot{\varepsilon}_i \neq 0$, by means of k_i, it follows from (G4) that $\dot{V}_i(t) \leqslant -c_i\beta_i p_i g_i \dot{\varepsilon}_i^{p_i-1}|s_i(t)|$, which means that the system trajectory is attracted to the sliding mainfold $s_i(t)=0$ within a finite time.

(2) When $\dot{\varepsilon}_i = 0$, it is meaningless to discuss the case that $s_i(t)=0$ since it shows the system trajectory has reached the sliding mainfold. If $s_i(t) \neq 0$, it can be obtained that $\varepsilon_i(t) \neq 0$ according to (6). Then, combined $\ddot{\varepsilon}_i$ with the control law (7), one can obtain that the point $(\varepsilon_i \neq 0, \dot{\varepsilon}_i = 0)$ is not the equilibrium point. This implies that the system state can not maintain at $\dot{\varepsilon}_i = 0$ and $\dot{V}_i(t)=0$ can not hold for $s_i(t) \neq 0$. When the system states change from $\dot{\varepsilon}_i = 0$ to $\dot{\varepsilon}_i \neq 0$, one can obtain from the first case that the system trajectory will be attracted to the sliding mainfold $s_i(t)=0$ by the PETM terminal sliding mode controller (7).

- When the system trajectory arrive at the practical sliding mode near $s_i = 0$, it can result in $\operatorname{sgn}\left(s_i\left(t_k^i\right)\right) \neq \operatorname{sgn}\left(s_i\left(t\right)\right)$. To illustrate this reason, without loss of generality, we assume $s_i\left(t_k^i\right) > 0$ at the instant $t = t_k^i$. According to (G2) and k_i, it can be obtained that $\dot{V}_i(t_k^i) < 0$. Then, the system trajectory will arrive at the sliding mainfold $s_i = 0$ and keep evolving until the next triggered instant. If $s_i\left(t_k^i\right) < 0$, one has $\dot{V}_i(t_k^i) < 0$ just as the case that $s_i\left(t_k^i\right) > 0$. Thus, the system trajectory will cross the sliding surface $s_i = 0$ and lead to $\operatorname{sgn}\left(s_i\left(t_k^i\right)\right) \neq \operatorname{sgn}\left(s_i\left(t\right)\right)$. Still, one can obtain that the system state will remain in a region called sliding band, namely practical sliding mode. From (6), it yields

$$\left|s_i\left(t\right) - s_i\left(t_k^i\right)\right| \leqslant \left|\varepsilon_i\left(t\right) - \varepsilon_i\left(t_k^i\right)\right| + \left|\beta_i\dot{\varepsilon}_i^{p_i}\left(t\right) - \beta_i\dot{\varepsilon}_i^{p_i}\left(t_k^i\right)\right|. \tag{G5}$$

According to the triggered condition (3), we have

$$\left|\varepsilon_i\left(t\right) - \varepsilon_i\left(t_k^i\right)\right| \leqslant \gamma_i\bar{\delta}_i + \bar{\delta}_{i+1}. \tag{G6}$$

Since $\dot{\varepsilon}_i^{p_i}(t)$ is Lipschitz continuous with a constant L_3^i, we obtain

$$\left|\beta_i\dot{\varepsilon}_i^{p_i}\left(t\right) - \beta_i\dot{\varepsilon}_i^{p_i}\left(t_k^i\right)\right| \leqslant \beta_i L_3^i\left\|\Xi_i\left(t\right) - \Xi_i\left(t_k^i\right)\right\| \leqslant \beta_i L_3^i\sqrt{\sum_{j=i-1}^{i+1}\bar{\delta}_j^2}, \tag{G7}$$

where $\Xi_i\left(t\right) = \left[\xi_{i-1}\left(t\right), \xi_i\left(t\right), \xi_{i+1}\left(t\right)\right]$. Then, the maximal size of sliding band can be obtained as

$$\left|s_i\left(t\right) - s_i\left(t_k^i\right)\right| \leqslant \gamma_i\bar{\delta}_i + \bar{\delta}_{i+1} + \beta_i L_3^i\sqrt{\sum_{j=i-1}^{i+1}\bar{\delta}_j^2}. \tag{G8}$$

In the following, the stability of closed-loop vehicular platoon system is studied. According to the sliding mainfold (6), it yields $\dot{\varepsilon}_i = \left(\frac{1}{\beta_i}\left(s_i - \varepsilon_i\right)\right)^{\frac{1}{p_i}}$. Then, by means of (G8), the ultimately boundedness of coupled quadratic spacing error can be derived as follows.

Appendix G.2 Ultimate boundedness of coupled quadratic spacing error

Proof. Consider a Lyapunov function candidate $\bar{V}_i\left(t\right) = \frac{1}{2}\varepsilon_i^2\left(t\right)$. According to (G8), the derivative of $\bar{V}_i\left(t\right)$ can be obtained as $\dot{\bar{V}}_i\left(t\right) = \varepsilon_i\left(\frac{1}{\beta_i}\left(s_i - \varepsilon_i\right)\right)^{\frac{1}{p_i}}$. It is seen that $\dot{\bar{V}}_i\left(t\right) < 0$ when the coupled quadratic spacing error $\varepsilon_i(t)$ stays in the two domains: $\Psi_1^i \triangleq \left\{\varepsilon_i > 0\left|\varepsilon_i > |s_i|\right.\right\}$ and $\Psi_2^i \triangleq \left\{\varepsilon_i < 0\left|\varepsilon_i < -|s_i|\right.\right\}$. It means that the coupled quadratic spacing error is attracted to the domain $\Psi_3^i = \left\{\varepsilon_i\left||\varepsilon_i| < |s_i|\right.\right\}$. By sorting to (G8), one can yield that $\varepsilon_i(t)$ converges to Ψ_i defined in Theorem 2. The proof is thus completed.

Appendix G.3 String stability

From Appendix F.2, the coupled quadratic spacing error $\varepsilon_i(t)$ will converge to a small region around the origin by setting appropriate parameters, and then the string stability of closed-loop system can be proved as follows.

Proof. From Appendix F.2, we know that $\varepsilon_i(t)$ can converge to a small region around the origin by setting appropriate parameters. Since $\varepsilon_i = \gamma_i e_i - e_{i+1}$ for $i < N$, it can be obtained as

$$e_{i+1}/e_i \approx \gamma_i. \tag{G9}$$

If $\gamma_i \in (0, 1]$ holds, one has

$$0 < |e_{i+1}|/|e_i| \approx \gamma_i \leqslant 1 \tag{G10}$$

Thus, we can obtain $|e_N(t)| \leqslant \left|e_{N-1}(t)\right| \leqslant \cdots \leqslant |e_1(t)|$, which implies that the closed-loop system is strong string stability. The proof is thus completed.

Appendix G.4 Traffic Flow Stability

It is obvious that the desired distance is achieved and the velocities of all vehicles are equal to v_0 at steady state, i.e., $d_i = \Delta_i$ and $v_i = v_0$ for all i. Thus, we have

$$\Delta_i = l_i + q_i v_0 + \frac{r_i}{2}v_0^2. \tag{G11}$$

Then, the steady state density can be obtained as

$$\rho_i = \frac{1}{l_i + q_i v_0 + \frac{r_i}{2}v_0^2}. \tag{G12}$$

Since the flow rate is defined as $Q_i(\rho_i) = \rho_i v_i$, we have

$$Q_i(\rho_i) = \rho_i\left(\sqrt{\frac{q_i^2}{r_i^2} - \frac{2l_i}{r_i} + \frac{2}{r_i\rho_i}} - \frac{q_i}{r_i}\right). \tag{G13}$$

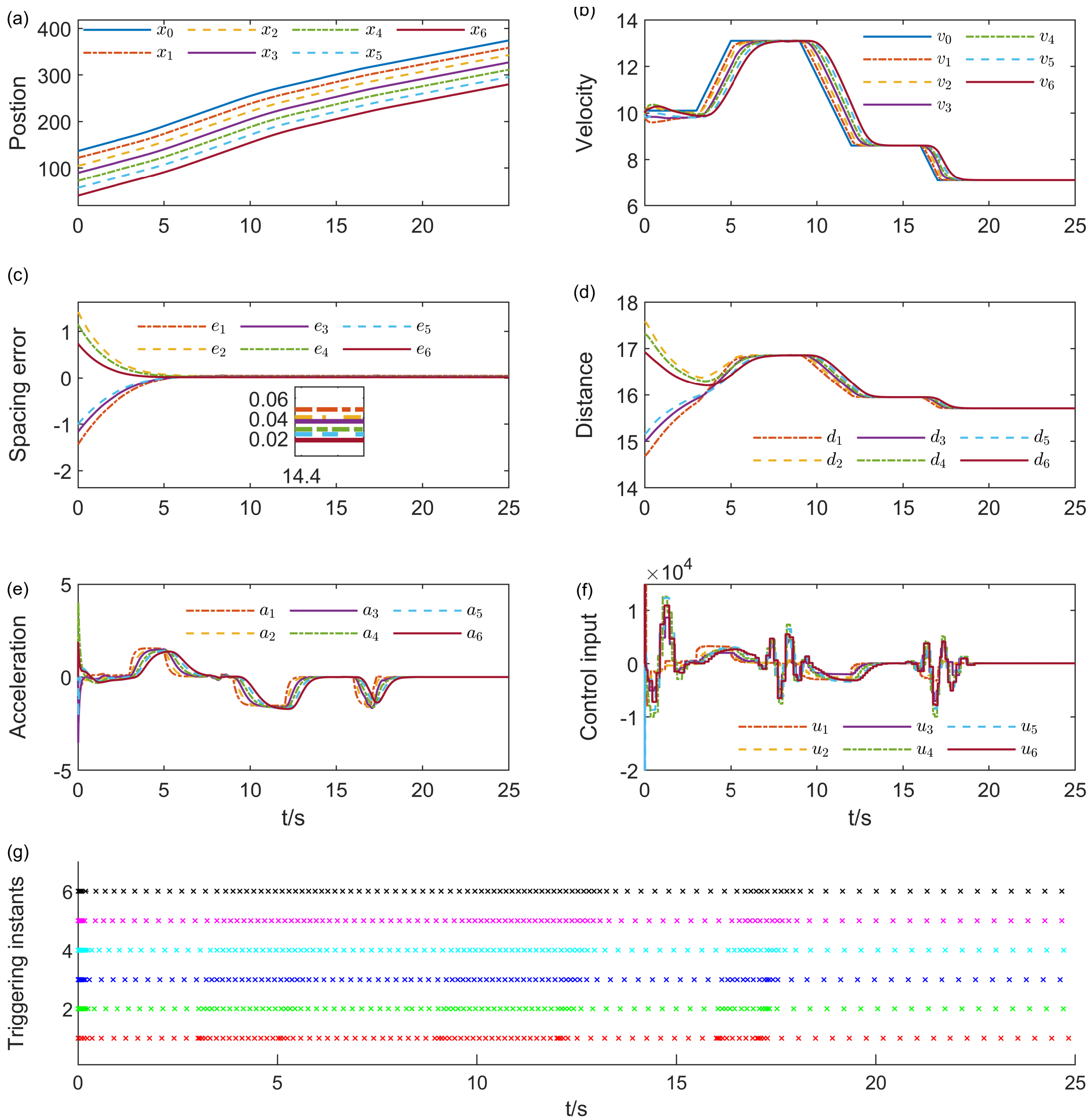

Figure G1 System trajectories under the PETM-based nonsingular terminal sliding mode controller.

To analyze the traffic flow stability of the proposed policy (5), the gradient $\partial Q_i/\partial \rho_i$ should be calculated. One has

$$\begin{aligned}\frac{\partial Q_i}{\partial \rho_i} = &\left(\sqrt{\frac{q_i^2}{r_i^2} - \frac{2l_i}{r_i} + \frac{2}{r_i\rho_i}} - \frac{q_i}{r_i}\right)\\ &- \frac{1}{r_i\rho_i\left(\sqrt{\frac{q_i^2}{r_i^2} - \frac{2l_i}{r_i} + \frac{2}{r_i\rho_i}}\right)}.\end{aligned} \tag{G14}$$

Then, the maximum traffic flow $\bar{\rho}_i$ can be obtained by $\partial Q_i/\partial \rho_i = 0$, which is given as follows

$$\bar{\rho}_i = \frac{1}{2l_i + q_i\sqrt{\frac{2l_i}{r_i}}}. \tag{G15}$$

The maximum traffic flow $\bar{\rho}_i$ also denotes the boundary between stable and unstable traffic flow.

Remark 3. In $g_i\left(t_k^i\right) = q_i + r_i v_i\left(t_k^i\right)$, the parameters q_i and r_i are positive, and g_i is equal to 0 only when the velocity v_i is less than 0, which violates Assumption 2.

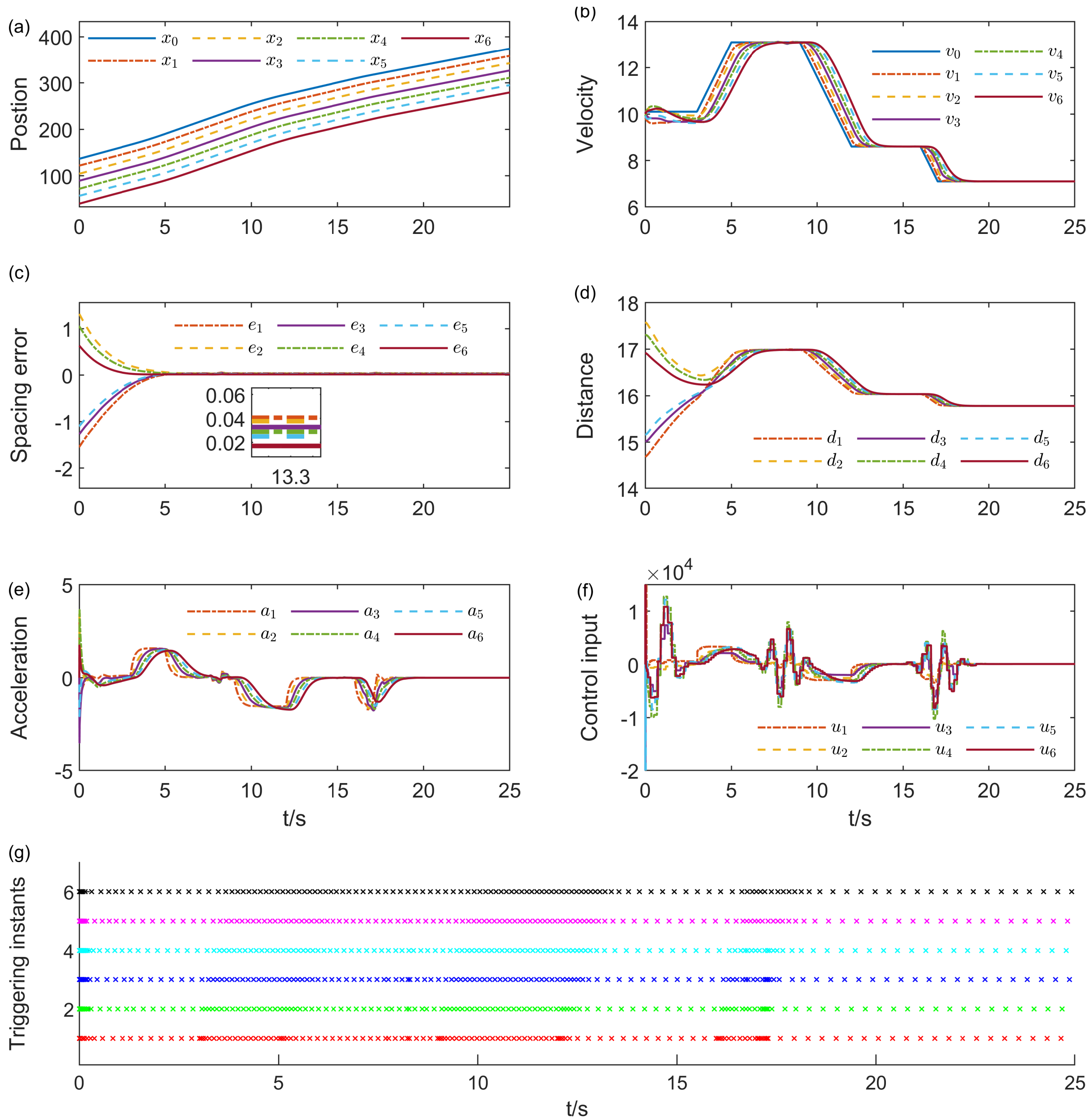

Figure G2 System trajectories under the SETM-based nonsingular terminal sliding mode controller.

Table G1 The parameters for vehicle i

i	1	2	3	4	5	6
m_i	2000	1700	1300	1900	2100	1900
τ_i	0.12	0.12	0.13	0.14	0.11	0.13
ν_i	1.2	1.19	1.21	1.18	1.2	1.22
A_i	2.21	2.19	2.2	1.98	1.95	2.18
C_{di}	0.35	0.4	0.39	0.38	0.34	0.33
d_{mi}	50	60	65	70	58	56

Table G2 The initial states for each vehicle i

i	0	1	2	3	4	5	6
$x_i(0)$	136.7	122.0	104.4	89.4	72.1	56.9	40.0
$v_i(0)$	10.1	9.8	10.0	10.1	9.9	9.9	10.0

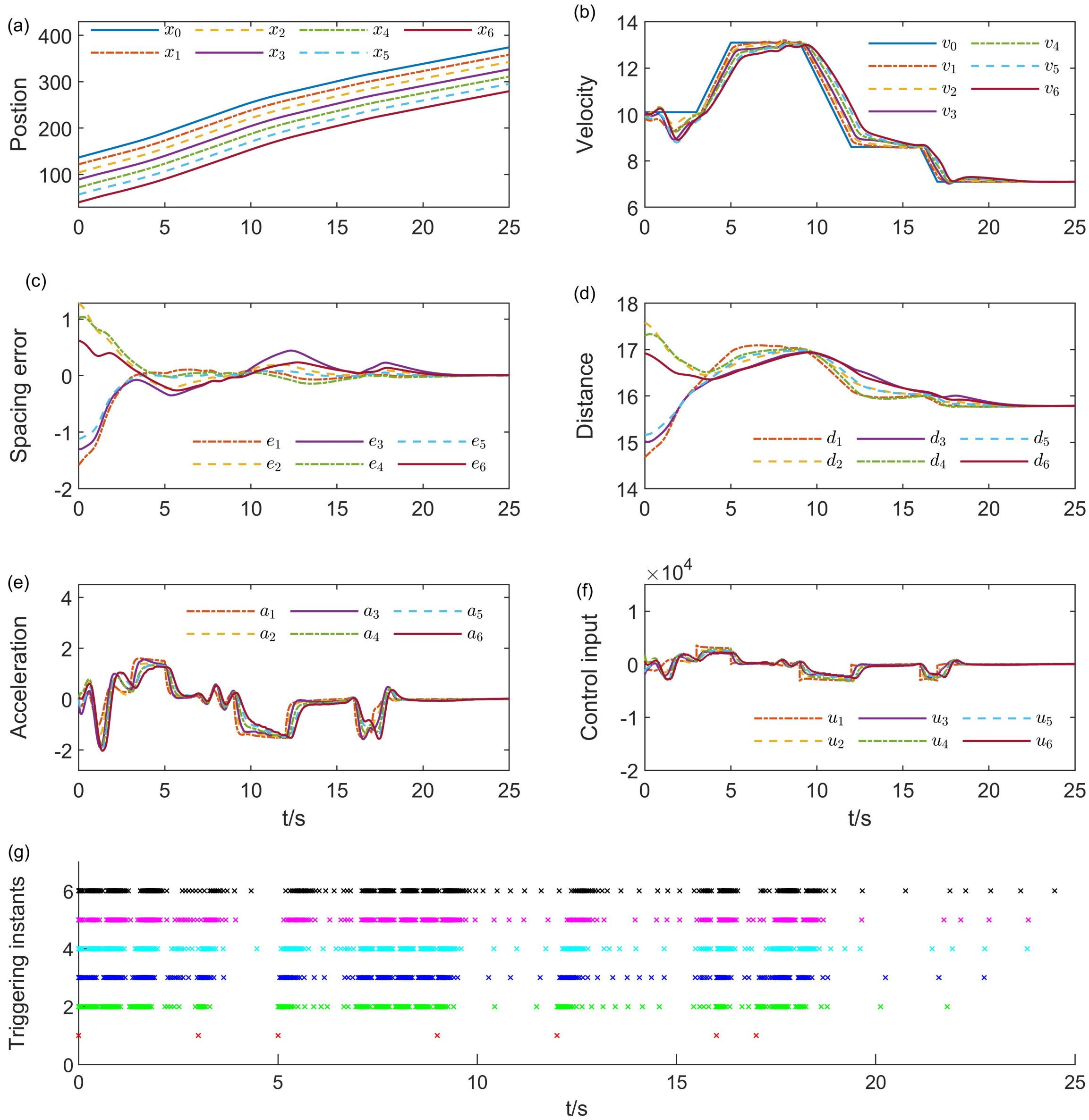

Figure G3 System trajectories under the controller in [2] without SMC.

Appendix H Simulation results

In this appendix, a numerical example is provided to demonstrate the effectiveness and efficiency of the proposed PETM-based nonsingular terminal sliding mode controller via computer simulations. In the simulations, We consider a vehicular platoon system consisting of 7 vehicles. The initial velocity and position of the leader are set as 10.1 m/s and 136.7 m respectively. The acceleration of the leader is given as

$$a = \begin{cases} 1.5m/s^2, & 3s \leqslant t < 5s \\ -1.5m/s^2, & 9s \leqslant t < 12s \\ -1.5m/s^2, & 16s \leqslant t < 17s \\ 0, & otherwise \end{cases}. \tag{H1}$$

For the coupled quadratic spacing policy, the minimum standstill l_i is 15m, the time delay q_i is 0.05s, and r_i is set as 0.014. The other parameters and the initial states for each vehicle are given in Table I and Table II respectively. In the PFESO, the parameters k_j^i, α_i and ε are determined by: $k_1^i = -12.25, k_2^i = -35.3, k_3^i = -50, k_4^i = -24.1, \alpha_i = 0.75$ and $\varepsilon = 0.2$. Then, in the

PETM-based terminal sliding mode controller, we assign $\beta_i = 2, p_i^1 = 11, p_i^2 = 7, \gamma_i = 0.9, k_i = 40, \bar{\delta}_i = 0.5$ and $\lambda_i = 0.05$. The external disturbance is set as $w_i = 52.5\sin(4t-3i)\,e^{-(t-0.7)^2} + 30\sin(6t+24)\,e^{-(t-8)^2} + +30\sin(6t-30)\,e^{-(t-17)^2}$. To further demonstrate the effectiveness and efficiency of the proposed control scheme, the comparison results are given in three different scenarios: (1) PETM with NTSMC, (2) ETM with NTSMC, (3) ETM without NTSMC which proposed in [2].

(i) *Verify the proposed control scheme.*

The simulation results under the PFESO (4) and PETM-based nonsingular terminal sliding mode controller (7) are shown in Fig.G1. Since there is no cross and overlapped position in Fig.G1(a), no collisions happens in both the steady-state condition and initial transient. Because of the coupled quadratic spacing policy, the inter-vehicle distance $d_i(t)$ increases along with velocity $v_i(t)$ in Fig.G1(b) and Fig.G1(d), meanwhile, the velocities of all consecutive vehicles converge to the leader velocity $v_0(t)$. Since all velocities are greater than zero, there is no reversing phenomenon in the simulation. It can be seen from Fig.G1(c) that the spacing error of each vehicle converges to zero in a finite time, and the spacing errors decrease along the vehicular platoon (i.e., $|e_6(t)| \leqslant |e_5(t)| \leqslant \cdots \leqslant |e_1(t)|$), which verifies the string stability of the closed-loop system. The acceleration $a_i(t)$ is shown in Fig.G1(e), which depicts that the acceleration of the vehicles are relatively smooth. Fig.G1(f) represents the engine input. In the Fig.G1(g), the ordinate represents the tag number of each vehicle and abscissa represents the transmission instants between vehicle and neighbors. For clarity, only the estimation results of the 4th and 6th followers' disturbance are shown in Fig.H1(a) and (b), which depicts that the external disturbance w_4 and w_6 are estimated effectively by the proposed PFESO.

(ii) *Comparison of the PETM and ETM with the NTSMC.*

For comparison of the SETM and PETM, the comparative simulations are depicted in Fig.G2. The position, velocity, spacing error, distance, acceleration and control input are similar to those in Fig.G1, so they are omitted here. From the comparative simulations, it can find that 759 and 853 sampled data are transmitted within 25s by the PETM and SETM. One can conclude that that the PETM-based nonsingular terminal sliding mode control can alleviate the communication and measurement burden while maintaining a satisfactory control performance.

(iii) *Comparison of the ETM with/without NTSMC.*

Fig.G3 depicts the responses of the ETM without NTSMC proposed in [2]. From Fig.G3, the position, velocity, distance, acceleration and control input are within acceptable levels respectively. Comparison of the simulation results of Fig.G2 (c) and Fig.G3 (c) shows that the external disturbances degrade the convergence rate of the controller without NTSMC, which demonstrates that the NTSMC can significantly enhance the anti-interference capability of the ETM systems.

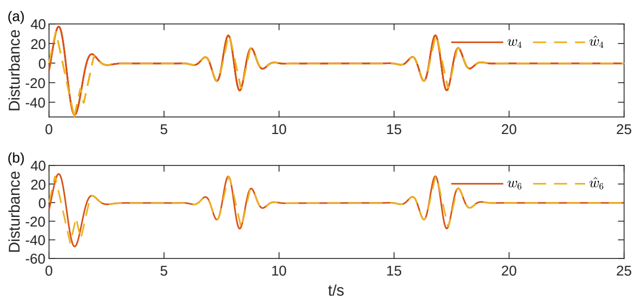

Figure H1 Estimation results of the disturbances via the PFESO.

References

1 Dolk V S, Ploeg J, Heemels W P M H. Event-triggered control for string-stable vehicle platooning. IEEE Trans Intell Transp Sys, 2017, 18: 3486-3500

2 Wang J, Ma F, Yang Y, et al. Adaptive event-triggered platoon control under unreliable communication links. IEEE Trans Intell Transp Sys, 2020, 23: 1924-1935

3 Song J, Wang Y K, Niu Y, et al. Periodic event-triggered terminal sliding mode speed control for networked PMSM system: A GA-optimized extended state observer approach. IEEE/ASME Trans Mechatr, 2022, 27: 4153-4164

4 Wen S, Guo G, Chen B, et al. Cooperative adaptive cruise control of vehicles using a resource-efficient communication mechanism. IEEE Trans Intell Veh, 2018, 4: 127-140

5 Ge X, Xiao S, Han Q L, et al. Dynamic event-triggered scheduling and platooning control co-design for automated vehicles over vehicular ad-hoc networks. IEEE/CAA Journ Autom Sin, 2021, 9: 31-46

6 Dou R, Ling Q. Model-based periodic event-triggered control strategy to stabilize a scalar nonlinear system. IEEE Trans Sys, Man, Cyber: Sys, 2019, 51: 5322-5335

7 Strijbosch N, Dullerud G E, Teel A R, et al. $\mathcal{L}_2$-Gain Analysis of Periodic Event-Triggered Control and Self-Triggered Control Using Lifting. IEEE Trans Autom Contr, 2020, 66: 3749-3756

8 Zheng S, Shi P, Agarwal R K, et al. Periodic event-triggered output regulation for linear multi-agent systems. Automatic, 2020, 122: 109223

9 Linsenmayer S, Dimarogonas D V, Allgwer F. Periodic event-triggered control for networked control systems based on non-monotonic Lyapunov functions. Automatic, 2019, 106: 35-46

10 Guo X G, Wang J L, Liao F, et al. CNN-based distributed adaptive control for vehicle-following platoon with input saturation. IEEE Trans Intell Transp Sys, 2017, 19: 3121-3132

11 Guo X, Wang J, Liao F, et al. Neuroadaptive quantized PID sliding mode control for heterogeneous vehicular platoon with unknown actuator deadzone. Internat Journ Rob Non Contr, 2019, 29: 188-208

12 Wang J, Luo X, Wang L, et al. Integral sliding mode control using a disturbance observer for vehicle platoons. IEEE Trans Indust Elect, 2019, 67: 6639-6648
13 Wang J, Luo X, Yan J, et al. Distributed integrated sliding mode control for vehicle platoons based on disturbance observer and multi power reaching law. IEEE Trans Intell Transp Sys, 2020, 23: 3366-3376
14 Zheng X, Luo X, Wang J, et al. Acceleration-feedback-based finite-time platoon control for interconnected vehicular system. Comput Elect Engin, 2022, 101: 108054
15 Yao D, Li H, Lu R, et al. Distributed sliding-mode tracking control of second-order nonlinear multiagent systems: An event-triggered approach. IEEE Trans Cyber, 2020, 50: 3892-3902
16 Behera A K, Bandyopadhyay B, Yu X. Periodic event-triggered sliding mode control. Automatic, 2018, 96: 61-72
17 Song J, Wang Y K, Niu Y, et al. Periodic event-triggered terminal sliding mode speed control for networked PMSM system: A GA-optimized extended state observer approach. IEEE/ASME Trans Mecha, 2022, 27: 4153-4164
18 Junejo A K, Xu W, Mu C, et al. Adaptive speed control of PMSM drive system based a new sliding-mode reaching law. IEEE Trans Pow Elect, 2020, 35: 12110-12121
19 Yan K, Chen M, Wu Q, et al. Extended state observer?based sliding mode fault?tolerant control for unmanned autonomous helicopter with wind gusts. IET Contr Theory Appl, 2019, 13: 1500-1513
20 Guo B Z, Jin F F. Sliding mode and active disturbance rejection control to stabilization of one-dimensional anti-stable wave equations subject to disturbance in boundary input. IEEE Trans Aut Contr, 2012, 58: 1269-1274
21 Tang S, Zhang L, Qian S, et al. Second-order sliding mode attitude controller design of a small-scale helicopter. Sci China Inf Sci, 2016, 59: 112209
22 Yang F, Shao X, Muyeen S M, et al. Disturbance observer based fractional-order integral sliding mode frequency control strategy for interconnected power system. IEEE Trans Pow Syst, 2021, 36: 5922-5932
23 Guo B Z, Zhao Z L. On convergence of non-linear extended state observer for multi-input multi-output systems with uncertainty. IET Control Theor Appl, 2012, 6: 2375-2386
24 Liu L, Wang D, Peng Z. State recovery and disturbance estimation of unmanned surface vehicles based on nonlinear extended state observers. Ocean Engin, 2019, 171: 625-632
25 Pukdeboon C. Extended state observer-based third-order sliding mode finite-time attitude tracking controller for rigid spacecraft. Sci China Inf Sci, 2019, 62: 1-16
26 Huang Y, Wang J, Shi D, et al. Toward event-triggered extended state observer. IEEE Trans Aut Cont, 2017, 63: 1842-1849
27 Ploeg J, Shukla D P, Van De Wouw N, et al. Controller synthesis for string stability of vehicle platoons. IEEE Trans Intell Transp Sys, 2013, 15: 854-865
28 Li K, Wang J, Zheng Y. Cooperative formation of autonomous vehicles in mixed traffic flow: Beyond platooning. IEEE Trans Intell Transp Sys, 2022, 23: 15951-15966
29 Li S E, Qin X, Zheng Y, et al. Distributed platoon control under topologies with complex eigenvalues: Stability analysis and controller synthesis. IEEE Trans Contr Sys Tech, 2017, 27: 206-220
30 Xing H, Ploeg J, Nijmeijer H. Robust CACC in the presence of uncertain delays. IEEE Tran Veh Tech, 2022, 71: 3507-3518
31 Guo G, Li P, Hao L Y. A new quadratic spacing policy and adaptive fault-tolerant platooning with actuator saturation. IEEE Trans Intell Transp Sys, 2020, 23: 1200-1212
32 Sungu H E, Inoue M, Imura J. Nonlinear spacing policy based vehicle platoon control for local string stability and global traffic flow stability. In: European Control Conference (ECC), Linz, 2015: 3396-3401
33 Guo G, Li P, Hao L Y. Adaptive fault-tolerant control of platoons with guaranteed traffic flow stability. IEEE Trans Veh Tech, 2020, 69: 6916-6927
34 He Q, Liu J K. Sliding mode observer for a class of globally Lipschitz non-linear systems with time-varying delay and noise in its output. IET Control Theor Appl, 2014, 8: 1328-1336
35 Guo B Z, Zhao Z. On the convergence of an extended state observer for nonlinear systems with uncertainty. Sys Contr Lett, 2011, 60: 420-430
36 Bhat S P, Bernstein D S. Geometric homogeneity with applications to finite-time stability. Mathemat Contr Sign Sys, 2005, 17: 101-127
37 Rosier L. Homogeneous Lyapunov function for homogeneous continuous vector field. Sys Contr Lett, 1992, 19: 467-473
38 Yiguang H, Zhongping J, Gang F. Finite-time input-to-state stability and related Lyapunov analysis. In: Chinese Control Conference, Zhangjiajie, 2007. 652-656
39 Ge X, Han Q L, Ding L, et al. Dynamic event-triggered distributed coordination control and its applications: A survey of trends and techniques. IEEE Trans Sys, Man, Cyber: Sys, 2020, 50: 3112-3125